2D Metal-Organic Frameworks Based Optoelectronic Neuromorphic Transistors for Human Emotion-Simulation and Neuromorphic Computing

Dapeng Liu[1], Qianqian Shi[1], Junyao Zhang[1], Li Tian[1], Lize Xiong[1], Shilei Dai[1], and Jia Huang[1]

[1]Affiliation not available

June 15, 2022

Abstract

Two-dimensional metal-organic frameworks (2D-MOFs) have been extensively studied as promising materials in the fields of eletrocatalysis, drug delivery, electronic devicese, etc. However, few studies have explored the application potential of 2D-MOFs in novel neuromorphic computing devices. In this work, we report an optoelectronic neuromorphic transistor based on a 2D-MOFs/polymer charge-trapping layer. We found that, the large specific surface area, stable crystal structure, and highly accessible active sites in 2D-MOFs make them excellent charge-trapping materials for our devices, which are beneficial for mimicking the memory and learning functions observed in the organism's nervous systems. Different types of synaptic behaviors have been realized in our 2D-MOFs-based neuromorphic devices under stimuli signal, e.g., paired-pulse facilitation, excitatory post-synaptic current, short-term memory, and long-term memory. More interestingly, emotion-adjustable learning behavior was realized by changing the value of the source-drain voltage. This work can shed light on the application of 2D-MOFs in neuromorphic computing and will contribute to the further development of neuromorphic computing devices.

Corresponding authors Email: huangjia@tongji.edu.cn (Jia Huang)

1610419@tongji.edu.cn (Shilei Dai)

ToC Figure

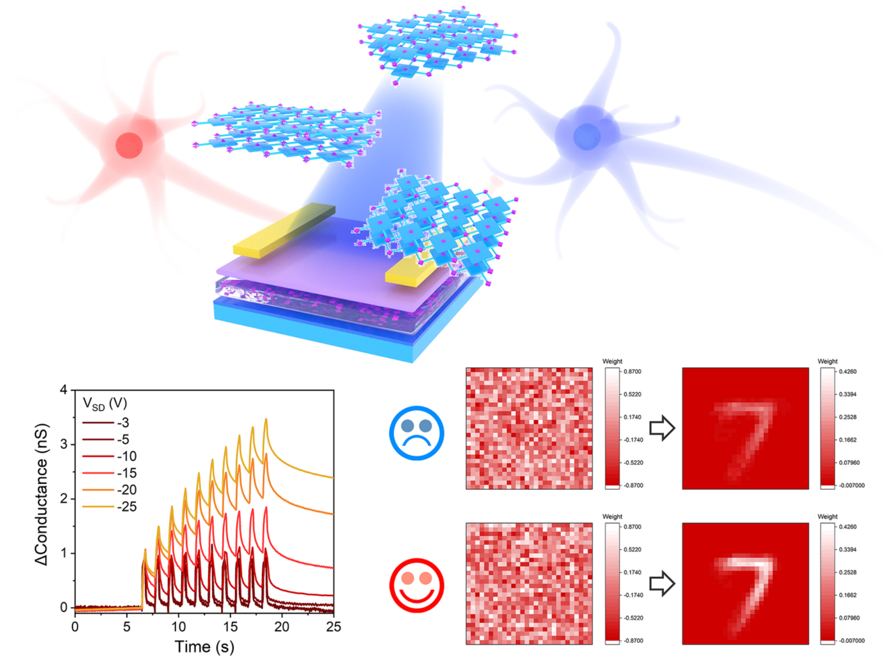

Figure 1: **Metal-organic framework** as a widely-studied material has been applied in many fields, such as catalysis, sensing, and energy storage. Here, an organic semiconductor/2D MOFs-polymer bi-layer was designed for optoelectronic neuromorphic transistors. The device displays excellent synaptic behaviors and unique emotional-tunable learning/forgetting properties, showing a promising application potential for neuromorphic systems.

Introduction

The explosion of information in the era of big data and the Internet of Things poses great challenges for von Neumann machines and sensors [1],[2],[3],[4],[5], requiring new computing paradigms to meet the requirements of energy efficiency and big data workloads. Hardware-based neuromorphic computing, which mimics the operating principles and architectures of the brain through physical devices, is considered as one of the most promising platforms for big data computing as it has the potential to provide lower neergy consumtpion and more efficient computing than the von Neumann machine in the future[6],[7],[8],[9]. So far, plenty of devices have been reported with synapse and neural-like functions[10],[11],[12], e.g., two-terminal memristors and three/multi-terminal transistors. Artificial neural networks based on an array of them have also been demonstrated for both low-level and high-level information processing[13],[14],[15],[16],[17],[18]. Among these neuromorphic devices, three/multi-terminal neuromorphic transistors have attracted much attention due to their high degree of control freedom, enabling many complex neural and synaptic functions, such as dendritic integration[19],[20],[21],[22]. Nonetheless, the development of three -terminal neuromorphic transistors is still in its infancy, and the capabilities of the devices need to be further expanded to achieve more interesting and useful applications.

On the other hand, in bio-synapse, the receptors on the surface of the post-membrane can be activated by transmitters released from the pre-membrane[23],[24],[25],[26]. The responsivity of the synapse to the stimulus depends on the receptor activity and the receptor number on the post-synaptic membrane. The illness of human emotions (mood disorders, depression, and stress)[27],[28],[29] usually influences the synaptic plasticity in the human brain, which would further influence the memory and learning behaviors of the human[30],[31],[32]. The emulation of the receptor-tuning synaptic behavior is essential for a detailed understanding of the mechanism of synaptic-behavior modulation. The multi-terminal regulation ability of neuromorphic transistors gives us the ability to simulate the human brain to learn emotional regulation, but there are few related research reports.

Two-dimensional metal-organic frameworks (2D-MOFs) with a periodic network structure are composed of metal clusters or metal ions and organic ligands[33],[34],[35]. The large specific surface area, stable crystal structure, and highly accessible active sites of 2D MOFs enable them with enormous application potential in a variety of fields, including catalysis, energy storage, gas separation, etc[36],[37],[38],[39],[40],[41],[42]. Recently, there are some reports about using MOFs as semiconducting materials and active layers for transistor and memory device fabrication, opening the door for using MOFs in electronic devices[43],[44],[45],[46]. However, few studies have explored the application potential of 2D-MOFs in optoelectronic neuromorphic computing devices.

Herein, we designed a 2D-MOFs/poly(methyl methacrylate) (PMMA) based optical-tunning dielectric layer for the fabrication of drain-tunable neuromorphic transistors. In addition to typical light-stimulated behaviors (paired-pulse facilitation (PPF) and excitatory postsynaptic current (EPSC)), the level of source-drain voltage can be utilized to model the number of receptors on the post-membrane and control the behavior of the device in response to prestimulation[47]. The emotion-dependent learning efficiency is also successfully demonstrated by our synaptic device via tuning the energy band alignment by changing the source-drain voltage (from -3 to -25 V). When the source-drain voltage (V_{DS}) is decreased to -1 V, the normal light-perception behavior of the device is completely depressed, which can be regarded as a human emotional illness. We also built a single-layer perceptron neural network based on the extracted parameters from our device, and demonstrate the emotion-tunable learning capability of the neural network. This work can not only broaden the application scenarios of 2D-MOFs but also further advance the development of neuromorphic electronics.

Experimental Methods

Materials Preparation

The 2D Zn_2(ZnTCPP) MOFs were synthesized according to the previous report. Tetrakis(4-carboxyphenyl)porphyrin (TCPP) was purchased from TCI Inc. and used without any further purification. TCPP and zinc nitrate ($Zn(NO_3)_2$) was dissolved in a mixed solvent (N, N-Dimethylformamide: ethanol = 3:1) and heated at 80 for 24 hours. Purple crystals can be observed after the sample was centrifugated at 4500 rpm for 10 min and washed with ethanol in 3 times. In order to obtain 2D Zn_2(ZnTCPP) MOFs, 20 mg of the as-prepared MOF (Zn_2(ZnTCPP)) was added to 4 mL chlorobenzene (CB) and was then sonicated using an ultrasonic bath machine filled with water. The temperature was maintained at 15-20. After the sonication, the resulted samples were centrifuged at 1500 rpm for 10 minutes to remove the large particles.

Device Fabrication

OFETs were fabricated using a silicon wafer with 300 nm silicon dioxide as substrate. 20 mg PMMA was added to the 1 mL 2D Zn_2(ZnTCPP) MOFs solution then was stirred for 6 hours to obtain a uniform solution. The solution was spin-coated on the washed substrate at 2000 rpm for 60 s. The pentacene was then thermally evaporated onto the 2D Zn_2(ZnTCPP) MOF-PMMA film at a rate of 0.1~0.3 Å/s. After that, 50 nm Au was thermally evaporated onto the pentacene film through a shadow mask as source-drain electrodes. The channel length and width were 30 µm and 1 mm, respectively.

Device Characterization

The surface morphology of pentacene and MOF-PMMA films were investigated by atomic force microscopy (Dimension Icon, Bruker). The thickness of 2D Zn_2(ZnTCPP) MOF-PMMA film was obtained from AFM. The device characteristics and synaptic behaviors measurement were carried out using a Keithley 4200-SCS instrument at room temperature. For the characterization of the synaptic phototransistors, a light source (white light, Thorlabs MCWHL5-C4) was used. The optical intensities were calibrated with an optical power meter (Thorlabs PM100D).

Results and Discussions

Materials Characterizations of 2D MOFs

The detailed fabrication processes of the 2D Zn_2(ZnTCPP) MOFs and the 2D-MOFs-based neuromorphic transistors are provided in the experimental section and Figure S1a. To prove that the Zn_2(ZnTCPP) MOF was successfully prepared, we performed X-ray photoelectron spectroscopy (XPS) to characterize the as-prepared materials. As shown in Figure S1b and d, the Zn 2p signal at ˜1017 eV and the N 1s signal at ˜399.7 eV were observed, respectively, and the C 1s signal consisted of three parts (-COOH, -C_2H_2, and -C_6H_6) was also been observed (Figure S1c). The signals of these elements of the as-prepared materials are in good agreement with those observed in Zn_2(ZnTCPP) MOFs reported in the literature[48]. In addition, X-ray powder diffraction (XRD) was also performed to characterize the as-prepared materials (Figure S2), which showed a similar XRD spectrum to the Zn_2(ZnTCPP) MOFs reported in the literature[31], further confirming that the as-prepared materials are Zn_2(ZnTCPP) MOFs. The bulk Zn_2(ZnTCPP) MOFs were further dispersed into 2D Zn_2(ZnTCPP) MOFs by using ultrasonication, and the sheet structure of the 2D Zn_2(ZnTCPP) MOFs was confirmed by the images from transmission-electron microscope (TEM) and atomic-force microscope (AFM) (Figure S3). 2D Zn_2(ZnTCPP) MOFs were mixed with polymethyl methacrylate (PMMA) and uniformly distributed in the PMMA film, as confirmed by the XPS with Ar ion etching technique (Figure S4).

Our optoelectronics neuromorphic transistors were fabricated by using the 2D Zn_2(ZnTCPP) MOFs -PMMA film as the charge trapping layer. The cross-section scanning-electron microscope (SEM) characterization of the device structure is shown in Figure S3b. The thickness of the charge trapping layer is about 30 nm. The thickness is consistent with the AFM results (Figure S5). The evaporated pentacene on the charge trapping layer displayed a typical island-growth layer-like structure, as shown in Figure S5c. To characterize the optical properties of the 2D Zn_2(ZnTCPP) MOFs -PMMA film and the pentacene film, we performed ultraviolet-visible spectroscopy (UV-vis) analysis, as shown in Figure S6a. The absorption peaks of the 2D Zn_2(ZnTCPP) MOFs -PMMA film and the pentacene film were located at ˜430 nm and ˜660 nm, respectively. The steady-state photoluminescence (PL) spectrums and the PL decay profiles of the 2D Zn_2(ZnTCPP) MOFs -PMMA film and the 2D Zn_2(ZnTCPP) MOFs -PMMA film/pentacene film were presented in Figure S6b and 6c. Compared with the 2D Zn_2(ZnTCPP) MOFs-PMMA/pentacene film, the 2D Zn_2(ZnTCPP) MOFs -PMMA film exhibited stronger emission peaks in the orange and red regions under excitation at 405 nm wavelength. The PL decay curve of the 2D Zn_2(ZnTCPP) MOFs-PMMA was well-fitted by a bi-exponential decay function, which presents two relaxation mechanisms, the lifetime of fast decay (τ_1) and short decay (τ_2). The fitting result can be quantified as $\tau_1 = 1.1$ ns and $\tau_2 = 6.7$ ns, respectively, while the profile of 2D Zn_2(ZnTCPP) MOFs-PMMA film/pentacene film exhibits a shorter decay time ($\tau_1 = 1.0$ ns and $\tau_2 = 4.6$ ns) due to the photo-induced charge transfer effect. Before the demonstration of the essential emotion-tunable neuromorphic functions, the basic synaptic behaviors of this device would be characterized at first.

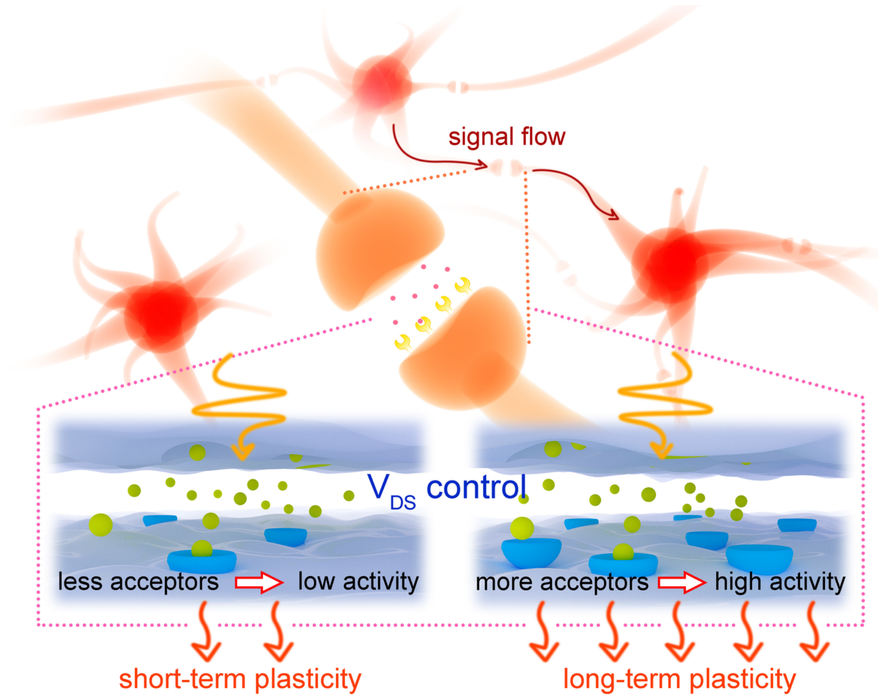

Figure 2: **The schematic illustration of the signal transmission behaviors is controlled by the receptor activities and receptor number.**

Basic Synaptic Performance of MOF-based Device

In the biological synapse, the external stimulus is transmitted and processed by neurons and synapses (**Figure 2**). The transmission rate of the signal flow depends on the number and the activity of the acceptors[49],[50]. Therefore, the post membrane with few and low-activity acceptors would induce a low post-synaptic current, which results in a weak signal response to the external stimulus. Compared with the low-activity synapse, the post membrane with more acceptors would trigger enhanced post-synaptic plasticity because more acceptors can be excited by the transmitters. The photo-responsiveness of our neuromorphic device can be controlled by the source-drain voltage (V_{DS}), which means that the effect of V_{DS} on synaptic devices is similar to that of the number of receptors on the postsynaptic membrane. Therefore, we can use V_{DS} to modulate our device performance.

Before demonstrating the V_{DS}-tunable neuromorphic device performance, we first characterized the basic synaptic transistor performance of the 2D MOF-based device (**Figure 3**, S7). In our device, the source-drain channel is regarded as the post-synaptic neuron, the I_{DS} is regarded as the post-synaptic signal and the channel conductance is treated as the synaptic weight. The photosensitive 2D Zn_2(ZnTCPP) MOFs-PMMA charge trapping layer can be regarded as a light-stimulated pre-synaptic neuron and the silicon gate can be regarded as an electrical-stimulated pre-synaptic neuron. In bio-synapse, the pre-synaptic neurons contain neurotransmitters and the post-synaptic neurons contain neurotransmitter receptors. The signal reached the pre-synaptic neuron would open the Ca^{2+} channel on the pre-synaptic membrane and therefore the membrane would release the neurotransmitters into the synaptic cleft[51],[52],[53]. The neurotransmitters in the synaptic cleft eventually interact with the neurotransmitter receptors to induce pre-synaptic signals transmission to post-synaptic neurons, triggering the EPSC and the IPSC[54]. The investigation of the EPSC behaviors with the light spike at various wavelengths ranging from 365 to 530 nm exhibits that the 430 nm light spike can induce the largest EPSC amplitude (Figure 3b), which is consistent with the UV-Vis spectrum of 2D Zn_2(ZnTCPP) MOFs-PMMA film (Figure 3b and Figure S6a). To assess the response of

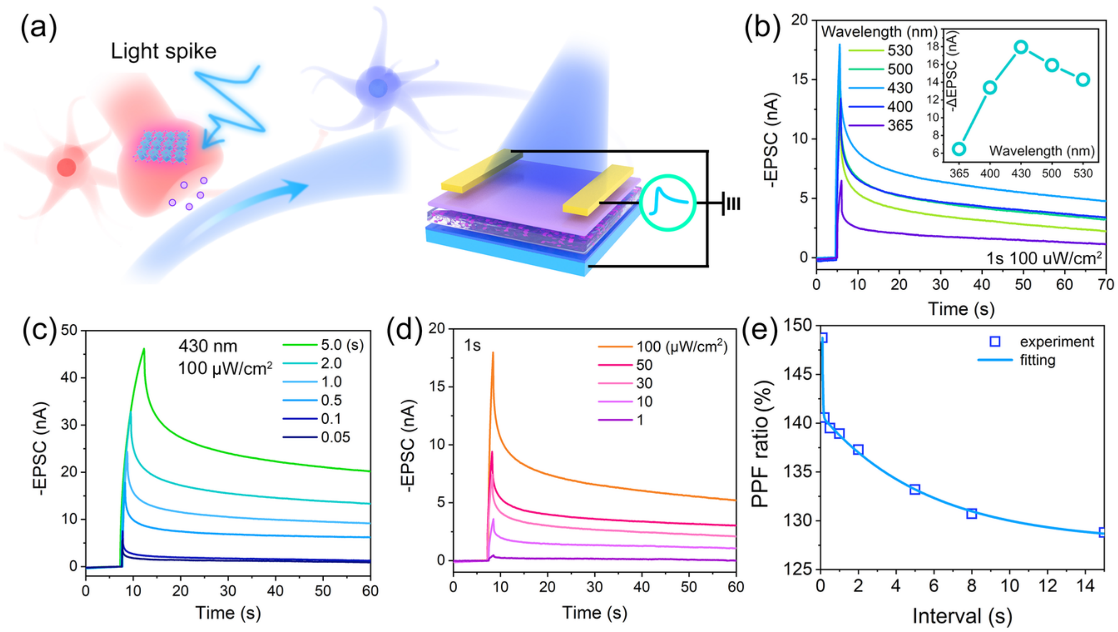

Figure 3: **Basic synaptic peroformance of the device.** (a) Schematics of the light-triggered bio-synapse and 2D-MOF-based neuromorphic transistors. (b) The synaptic response of our device to the light spikes with different wavelengths (inset, the change of the EPSC vs light wavelength). (c-d) The LTP or STP formation in our photonic synaptic device depends on the light-spike duration (λ= 430 nm, intensity: 100 μW/cm^2) and the light-spike intensity (λ= 430 nm, duration: 1 s). (e) The PPF ratios at various spike intervals.

our neuromorphic device to light stimulation (430 nm), we further investigated EPSCs with different light spike durations (Figure 3c) and intensities (Figure 3d), respectively. The EPSCs could be enhanced with the increment of light spike duration or intensity.

Paired-pulse facilitation (PPF) is an essential behavior in the bio-synaptic system for temporary information processing, where the post-synaptic conductance (synaptic weight) can be enhanced via two consecutive pre-synaptic stimulations, resulting in the device showing higher conductance after the second spike than that after the first spike[55]. To show that our device can simulate PPF behavior, a pair of optic-signal spikes with a certain spike interval was utilized as a pre-synaptic signal spike. As shown in Figure 3e, two consecutive 430 nm 100 μW/cm^2 light spikes (1 s) with 1 s interval were applied to our synaptic device. The larger value of the EPSC triggered by the 2$^{\text{nd}}$ light spike than that value triggered by the 1$^{\text{st}}$ light spike was observed. The PPF ratio can be defined by the following equation:

$$PPF\ ratio = \frac{A_2}{A_1} \times 100\%$$

where the values A_1 and A_2 are the EPSC amplitudes of the first and the second light spike, respectively. The PPF ratio would decrease when we increase the interval time (t_{inter}) (Figure 3e). The maximum value of the PPF is ~149%, which was obtained at the minimum t_{inter} of 100 ms. The electrons trapping in the 2D Zn_2(ZnTCPP) MOFs-PMMA layer induced by the first light spike have insufficient time to recombine with holes before the 2$^{\text{nd}}$ light spike was applied, which results in an enhanced EPSC amplitude after the second light spike. The PPF decay can be described as the combination of rapid decay and slow decay, defined by the following equation:

$$W = \frac{EPSC}{V_{DS}}$$

By changing the light spike parameters, we achieved the simulation of different types of synaptic plasticity in our 2D Zn_2(ZnTCPP) MOFs-based neuromorphic devices, suggesting the potential of our device for future neuromorphic computing applications.

Demonstration of Emotion-Tunable Simulation

Humans have abundant emotions (such as happy, sad, plain, mild), which are essential in human learning and memory. Positive emotion would improve vitality and enhance learning efficiency. By contrast, negative emotion would depress vitality, resulting in a low learning rate (**Figure 4a**)[56],[57],[58]. The V_{DS}-tunable photoresponse of our 2D Zn_2(ZnTCPP) MOFs-based neuromorphic device can be utilized to mimic emotion-tunable memory and learning behaviors. Figure 4b displays the energy alignment controlled by V_{DS} of the pentacene/2D Zn_2(ZnTCPP) MOFs-PMMA structure, which can be used to describe the mechanism of the V_{DS} tunning capability. The kelvin probe force microscope (KPFM) potential variation with the light illumination confirmed the hole accumulation in pentacene under illumination (Figure S7). The level of the V_{DS} determines the energy band structure. At high V_{DS}, the large energy difference between the drain electrode and gate electrode enhances the bending of the energy band in the pentacene and MOF layers. Light-generated carriers are easily transferred to the OSC channel, which results in a large ΔEPSC value. The recombination rate of the light-induced accumulated charge carriers in pentacene would be also depressed, delivering a long retention time. On the contrary, the recombination rate of light-generated carriers would be increased at a low V_{DS} level because of the weak bending of the energy band. Furthermore, at the ultra-low V_{DS} or even zero-level state, the transfer process of light-induced carriers would be in chaos.

The device tests were then carried out for a V_{DS}-tunning demonstration. In Figure 4c, the device current (I_{DS}) can be defined as the vitality of the neuron, where the red face means happy, the yellow face means mid and the blue face means sad. The pre-synaptic current value increases from 0.2 nA to 30 nA (sad, mild, and happy) when the V_{DS} increases from 0.1 V to 25 V, suggesting the V_{DS} can be used to modulate the "vitality" of our device. As shown in Figure 4d, 10 consecutive light spikes (0.3 s, 50 $\mu W/cm^2$) were applied to the device with various V_{DS} (different emotions, sad, mild, happy). The change of the device EPSC is enhanced with the increment of the V_{DS} and the device at the V_{DS} of -25 V exhibits the largest EPSC change (Figure 3e), while the level of the V_{DS} would not change the amplification of the conductance change in the first spike (inset, Figure 4e). When a human was sad (negative emotion, low V_{DS}), the synapse displays a low steady signal and low responsivity, resulting in a low A_{10}/A_1 ratio. Humans under positive emotions can efficiently process the information and enhance memory. A high A_{10}/A_1 ratio was observed in our neuromorphic device under high V_{DS} (happy) after 10 light spikes (Figure 4f). The retention time (memory) was also enhanced with the increment of V_{DS} (Figure 4g, h). The above results show the V_{DS}-tunable neuromorphic performance of the device was successfully achieved.

Emotion illness is a kind of psychiatric disorder such as depression, anxiety disorders, and schizophrenia, which has an adverse effect on human society. In the simulation of the human emotion with device V_{DS} level, the value range from -3 V to -25 V refers to the normal human emotions including happy, mild, and sad. When the V_{DS} is decreased to an ultralow level (-1 V and -0.1 V), the device exhibits irregular responses to the same 10 consecutive light stimuli (0.3 s, 50 $\mu W/cm^2$). The current enhancement is very weak and undesirable fluctuation can be observed (**Figure 5a**). Compared with the response of the device to light spikes under $V_{\mathrm{DS}} = -3$ V, the device exhibits abnormal responses. This stage of our device can be regarded as the synaptic unit in emotional illness. The damage of the depression in the human brain described in Figure 5b includes chaos, confusion, and irregular response to external stimuli. The external behaviors of the depression were successfully simulated by the current variations of our device to a certain degree.

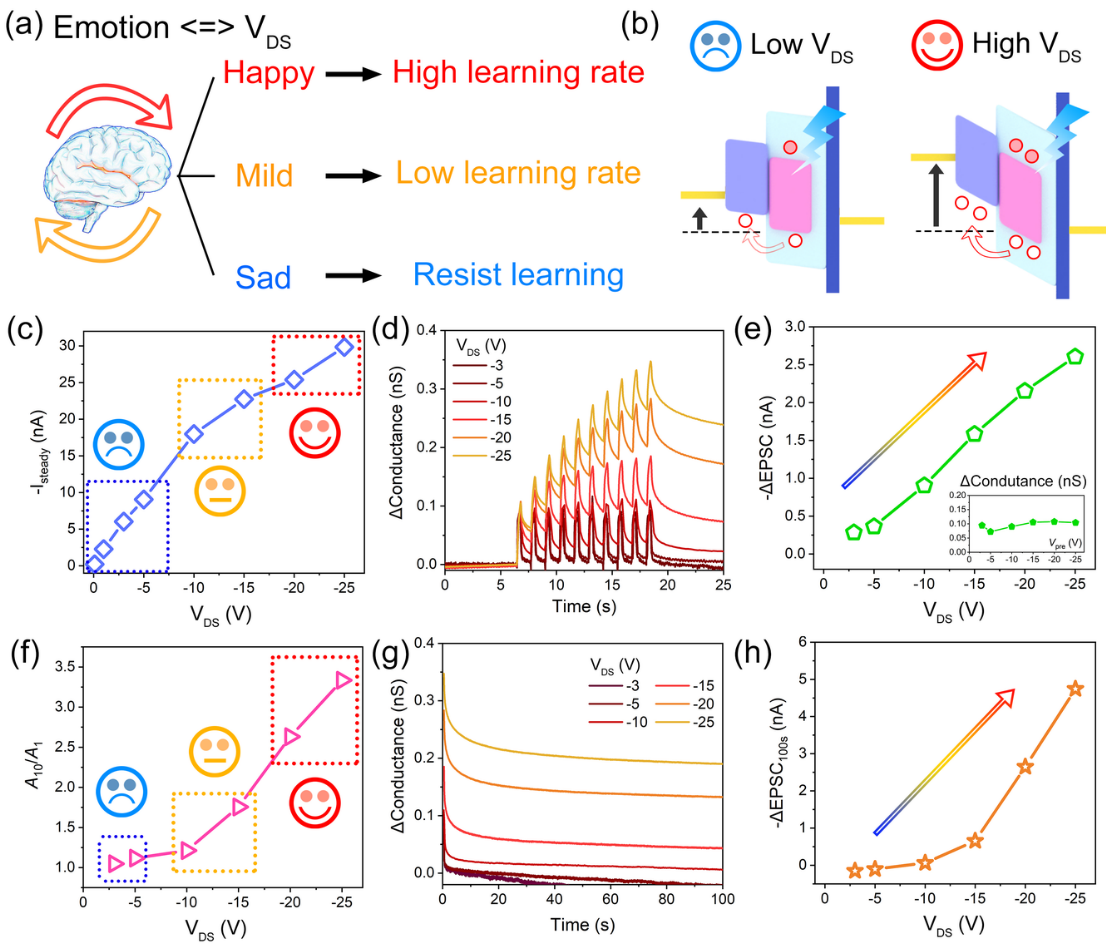

Figure 4: **The emotion simulation of the MOF-based device.** (a) The schematic illustration of emotion simulation via source-drain control. (b) The energy alignment of the pentacene/2D Zn_2(ZnTCPP) MOFs-PMMA structure with different V_{DS}. (c) The current value before learning under various V_{DS} (-3, -5, -10, -15, -20, -25 V). (d) The change of the channel conductance after 10 light spikes with various V_{DS}. (e) The EPSC change under the 1st light spike as a function of V_{DS} (inset, the change of the corresponding conductance). (f) The A_{10}/A_1 ratio and (g) state retention behavior under different $V_{DS.}$ (h) The change of EPSC after learning in 100 s with various V_{DS}.

The Emotion-SLP Simulation

For the further demonstration of the emotion-tunable learning capability of our device, we built a neural network based on single-layer perceptron (SLP) by using the extracted weight updating parameters from our neuromorphic device. We severe "emotion regulation" of SLP neural network learning capability by using the simulated neural network model to recognize modified national institute of MNIST handwritten digits after training. In **Figure 6a**, the network would consist of 784 input neurons (the resolution of the digits image is 28×28) and 10 output neurons (the labels was set from 0 to 9) The input neurons and the output neurons are fully connected through 784×10 synapse (the values are regarded as synaptic weights). The input neuron would receive one signal converted from the gray level in one pixel of the training image (28×28). Then the input vector (V_i) functions through the weight values in the synaptic network ($W_{i,j}$). The calculation result was converted and transmitted to the output vector with the utilization of the sigmoid activation

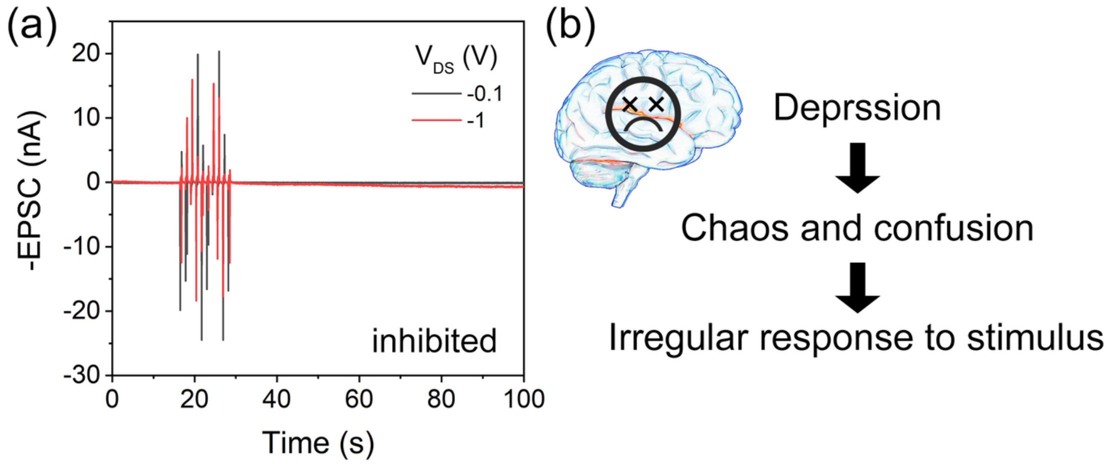

Figure 5: **The simulation of the emotion illness.** (a) The current response of the synaptic device to the 10-times 430 nm light spikes under various weak V_{DS} (-0.1 V and -1 V). (b) The schematic effect of the depression on the synaptic response to the external stimulus.

function. The difference between the image's label and the output value would determine the direction of the synaptic-weight updating process via the backpropagation algorithm. Therefore, in one batch, the SLP network was trained through the input of 60000 image. Then the recognition rate (RR) of the trained SLP network for 10 numbers from "0" to "9" was tested with 10000 testing images. The curves and their fitting curves for the 100-weight update under various emotions (V_{DS}, -5 V, -15 V) are shown in Figure 6b.

The parameters were obtained from the fitting curves, which would be applied in the following MNIST-based recognition simulation process. The recognition rate of the network was increased with the input process of training images (Figure 6c). The network under high V_{DS} (positive emotion) exhibits a higher recognition rate (~75%) than that under low V_{DS} (negative emotion, ~65%). The instability of the training process can be observed in a low-V_{DS} (negative emotion) network. Figure 6d illustrates the mapping of the corresponding conductances (W), which can recognize the digit "7" before and after training. It can be observed that the conductance mapping based on high V_{DS} (positive emotion) exhibits the more obvious pattern "7" than that based on low V_{DS} (negative emotion).

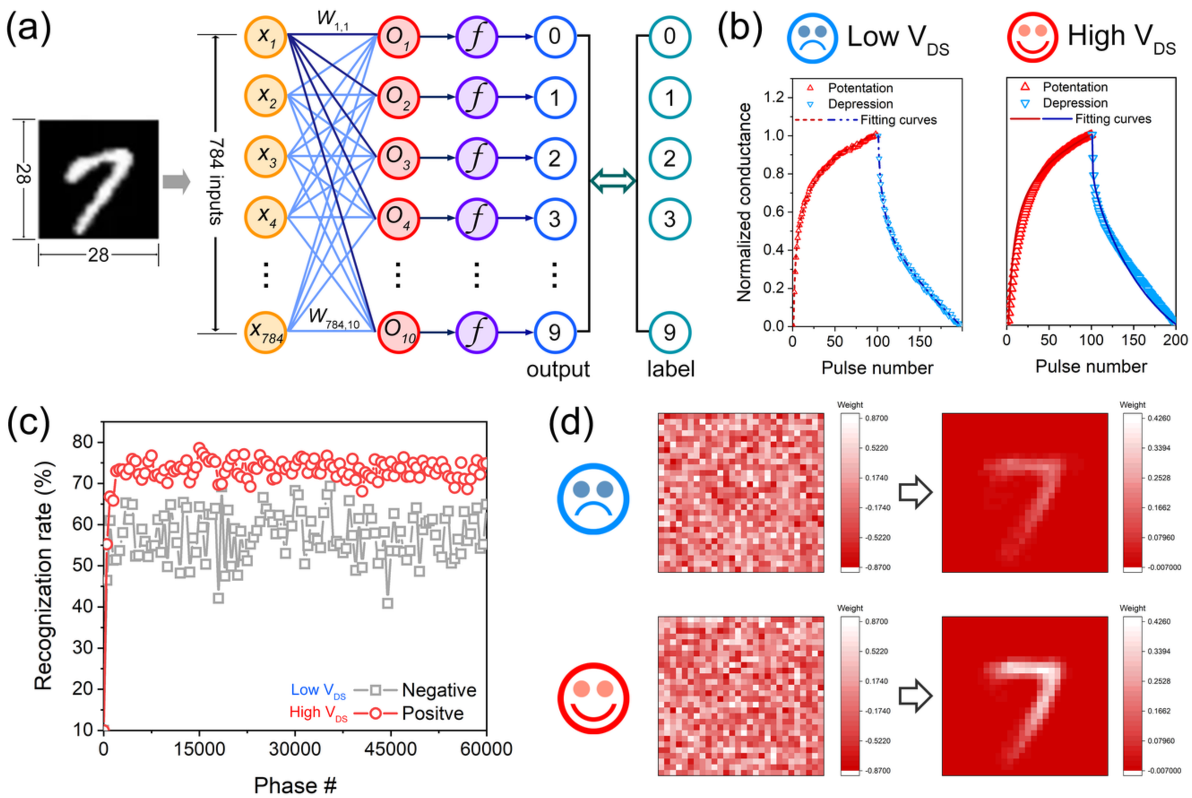

Figure 6: **Pattern recognition based on simulated neural network.** (a) The SLP network with 784 input neurons and 10 output neurons. (b) 200 levels of synaptic weights were obtained from the optical-pulse and electric-pulse trains of our synaptic transistor. (c) The recognition rate of the network with the increasement of training epochs. (d) The hotspot graphs of synaptic weights to recognize the number "3" under various emotions.

Conclusion

In this work, we have successfully demonstrated a novel optoelectronic neuromorphic transistor based on the design of the tunable energy band structure of the 2D MOFs-polymer/OSC layer. The 2D MOFs-polymer blended layer was used as the photo-sensing component and the uniformly dispersed 2D MOFs were used as the charge trapping centers. The generation, transportation, and trapping processes of the photogenerated charges on the 2D MOFs-polymer/OSC heterojunction provided the transistors with a variety of synaptic behaviors. More interestingly, we have successfully simulated human emotion-tunable learning and memory behaviors via changing the value of source-drain voltage. The study can shed light on the application of 2D-MOFs in neuromorphic computing and is also helpful to the further development of neuromorphic computing devices.

Acknowledgements

This work was supported by the Science and Technology Foundation of Shanghai (19JC1412402 and 20JC1415600), the National Natural Science Foundation of China (62074111), Shanghai Municipal Science and Technology Major Project (2021SHZDZX0100), Shanghai Municipal Commission of Science and

Technology Project (19511132101), and the support of the Fundamental Research Funds for the Central Universities. The authors are also thankful for the support of the Measurements and Analysis Center, School of Materials Science and Engineering, Tongji University.

Conflict of interest

The authors declare no conflict of interests.

References

[1]J. W. Lichtman, H. Pfister, N. Shavit, *Nature Neuroscience* **2014**, *17.*

[2]Y. van de Burgt, A. Melianas, S. T. Keene, G. Malliaras, *Nature Electronics* **2018**, *1.*

[3]H. L. Park, N. K. Y. Lee, D. G. Seo, G. T. Go, T. W. Lee, *Advanced Materials* **2020**, *32.*

[4]D. Hao, J. Zou, J. Huang, *InfoMat* **2020**, *2.*

[5]D. Liu, Q. Shi, S. Jin, Y. Shao, J. Huang, *InfoMat* **2019**, *1.*

[6]L. S. Smith, *Neuromorphic Systems: Past and Present and Future and in Advanced Materials*, Springer, **2010**.

[7]M. A. Zidan, J. P. Strachan, W. D. Lu, *Nature electronics* **2018**, *1.*

[8]R. F. Service, *Science* **2014**, *345.*

[9]S. Dai, Y. Zhao, Y. Wang, J. Zhang, L. Fang, S. Jin, Y. Shao, J. Huang, *Advanced Functional Materials* **2019**, *29.*

[10]N. K. Upadhyay, S. Joshi, and J. J. Yang, *Science China Information Sciences* **2016**, *59.*

[11]H. Markram, *Nature Reviews Neuroscience* **2006**, *7.*

[12]C. K. Machens, *Science* **2012**, *338.*

[13]Z. Lv, M. Chen, F. Qian, V. A. L. Roy, W. Ye, D. She, Y. Wang, Z.-X. Xu, Y. Zhou, S.-T. Han, *Advanced Functional Materials* **2019**, *29.*

[14]J. Sun, S. Oh, Y. Choi, S. Seo, M. J. Oh, M. Lee, W. B. Lee, P. J. Yoo, J. H. Cho, J.-H. Park, *Advanced Functional Materials* **2018**, *28.*

[15]J. Tang, F. Yuan, X. Shen, Z. Wang, M. Rao, Y. He, Y. Sun, X. Li, W. Zhang, Y. Li, B. Gao, H. Qian, G. Bi, S. Song, J. J. Yang, H. Wu, *Advanced Materials* **2019**, *31.*

[16]Z. Wang, M. Rao, J.-W. Han, J. Zhang, P. Lin, Y. Li, C. Li, W. Song, S. Asapu, R. Midya, Y. Zhuo, H. Jiang, J. H. Yoon, N. K. Upadhyay, S. Joshi, M. Hu, J. P. Strachan, M. Barnell, Q. Wu, H. Wu, Q. Qiu, R. S. Williams, Q. Xia, J. J. Yang, *Nature Communications* **2018**, *9.*

[17]S. Dai, X. Wu, D. Liu, Y. Chu, K. Wang, B. Yang, J. Huang, *ACS Applied Materials & Interfaces* **2018**, *10.*

[18]J. Zhang, Q. Shi, R. Wang, X. Zhang, L. Li, J. Zhang, L. Tian, L. Xiong, J. Huang, *InfoMat* **2021**, *3.*

[19]F. Xi, Y. Han, M. Liu, J. H. Bae, A. Tiedemann, D. Grützmacher, Q.-T. Zhao, *ACS Applied Materials & Interfaces* **2021**, *13*.

[20]S. Oh, T. Kim, M. Kwak, J. Song, J. Woo, S. Jeon, I. K. Yoo, H. Hwang, *IEEE Electron Device Letters* **2017**, *38*.

[21]A. I. Khan, A. Keshavarzi, S. Datta, *Nature Electronics* **2020**, *3*.

[22]Y. van de Burgt, E. Lubberman, E. J. Fuller, S. T. Keene, G. C. Faria, S. Agarwal, M. J. Marinella, A. A. Talin, A. Salleo, *Nature Materials* **2017**, *16*.

[23]R. S. Zucker, W. G. Regehr, *Annual Review of Physiology* **2002**, *64*.

[24]C. L. R. A. Nicoll, R. C. Malenka, D. Muller, *Nature Neuroscience* **2000**, *3*.

[25]R. C. Carroll, E. C. Beattie, M. von Zastrow, R. C. Malenka, *Nature Reviews Neuroscience* **2001**, *2*.

[26]G. L. Collingridge, J. T. R. Isaac, Y. T. Wang, *Nature Reviews Neuroscience* **2004**, *5*.

[27]R. S. Duman, *Molecular Psychiatry* **2002**, *7*.

[28]R. S. Duman, G. K. Aghajanian, G. Sanacora, J. H. Krystal, *Nature Medicine* **2016**, *22*.

[29]J. G. Howland, Y. T. Wang, *Chapter 8 Synaptic Plasticity in Learning and Memory: Stress Effects in the Hippocampus and in Progress in Brain Research*, Elsevier, **2008**.

[30]D. G. Rainnie, R. Bergeron, T. J. Sajdyk, M. Patil, D. R. Gehlert, A. Shekhar, *Journal of Neuroscience* **2004**, *24*.

[31]S. M. J. McBride, C. H. Choi, Y. Wang, D. Liebelt, E. Braunstein, D. Ferreiro, A. Sehgal, K. K. Siwicki, T. C. Dockendorff, H. T. Nguyen, T. V. McDonald, T. A. Jongens, *Neuron* **2005**, *45*.

[32]R. Ikeda, Y. Takahashi, K. Inoue, F. Kato, *Pain* **2007**, *127*.

[33]G. Ding, Y. Wang, G. Zhang, K. Zhou, K. Zeng, Z. Li, Y. Zhou, C. Zhang, X. Chen, S.-T. Han, *Advanced Functional Materials* **2019**, *29*.

[34]K. Sasitharan, D. G. Bossanyi, N. Vaenas, A. J. Parnell, J. Clark, A. Iraqi, D. G. Lidzey, J. A. Foster, *Journal of Materials Chemistry A* **2020**, *8*.

[35]S. Zhang, X. Pei, H. Gao, S. Chen, J. Wang, *Chinese Chemical Letters* **2020**, *31*.

[36]G. Ding, B. Yang, K. Zhou, C. Zhang, Y. Wang, J.-Q. Yang, S.-T. Han, Y. Zhai, V. A. L. Roy, Y. Zhou, *Advanced Electronic Materials* **2020**, *6*.

[37]Y. Liu, Y. Wei, M. Liu, Y. Bai, G. Liu, X. Wang, S. Shang, W. Gao, C. Du, J. Chen, Y. Liu, *Angewandte Chemie International Edition* **2021**, *60*.

[38]W. Zhao, J. Peng, W. Wang, S. Liu, Q. Zhao, W. Huang, *Coordination Chemistry Reviews* **2018**, *337*.

[39]J. Song, J. Zheng, A. Yang, H. Liu, Z. Zhao, N. Wang, F. Yan, *Materials Chemistry Frontiers* **2021**, *5*.

[40]Y. Gu, L. Miao, Y. Yin, M. Liu, L. Gan, L. Li, *Chinese Chemical Letters* **2021**, *32*.

[41]J. Zhang, Y. Wang, H. Wang, D. Zhong, T. Lu, *Chinese Chemical Letters* **2022**, *33*.

[42]S. Zheng, Y. Ru, H. Xue, H. Pang, *Chinese Chemical Letters* **2021**, *32*.

[43]L. Pan, Z. Ji, X. Yi, X. Zhu, X. Chen, J. Shang, G. Liu, R.-W. Li, *Advanced Functional Materials* **2015**, *25*.

[44]Y. Liu, H. Wang, W. Shi, W. Zhang, J. Yu, B. K. Chandran, C. Cui, B. Zhu, Z. Liu, B. Li, C. Xu, Z. Xu, S. Li, W. Huang, F. Huo, X. Chen, *Angewandte Chemie International Edition* **2016**, *55*.

[45]S. M. Yoon, S. C. Warren, B. A. Grzybowski, *Angewandte Chemie International Edition* **2014**, *53.*

[46]G. Wu, J. Huang, Y. Zang, J. He, G. Xu, *Journal of the American Chemical Society* **2017**, *139.*

[47]K. Tully, V. Y. Bolshakov, *Molecular Brain* **2010**, *3.*

[48]H. Ang, L. Hong, *ACS Applied Materials & Interfaces* **2017**, *9.*

[49]I. Pérez-Otaño, M. D. Ehlers, *Trends in Neurosciences* **2005**, *28.*

[50]M. Zoli, A. Jansson, E. Syková, L. F. Agnati, K. Fuxe, *Trends in Pharmacological Sciences* **1999**, *20.*

[51]J. Bockaert, S. Claeysen, C. Bécamel, A. Dumuis, P. Marin, *Cell and Tissue Research* **2006**, *326.*

[52]C. Guerrier, D. Holcman, *Frontiers in Synaptic Neuroscience* **2018**, *10.*

[53]A. Merighi, C. Salio, F. Ferrini, L. Lossi, *Journal of Chemical Neuroanatomy* **2011**, *42.*

[54]A. J. Smith, S. Owens, I. D. Forsythe, *The Journal of Physiology* **2000**, *529.*

[55]P. P. Atluri, W. G. Regehr, *The Journal of Neuroscience* **1996**, *16.*

[56]I. Boniwell, A. D. Tunariu, *Positive Psychology: Theory and Research and Applications*, McGraw-Hill Education, **2019**.

[57]E. M. Selhub, A. C. Logan, *Your Brain on Nature: The Science of Nature's Influence on Your Health and Happiness and Vitality*, John Wiley & Sons, **2012**.

[58]L. Li, A. D. I. Gow, J. Zhou, *Mind, Brain, and Education* **2020**, *14.*